PCCP

Accepted Manuscript

ROYAL SOCIETY OF CHEMISTRY

rsc.li/pccp

View Article Online
DOI: 10.1039/C7CP04817C

Journal Name

ARTICLE

Highly Stable Graphene Oxide-Gold Nanoparticle Platforms for Biosensing Applications

Received 00th January 20xx,
Accepted 00th January 20xx

DOI: 10.1039/x0xx00000x

www.rsc.org/

Dania Hernández-Sanchez,[a,b] Giovanny Villabona-Leal,[a] Izcoatl Saucedo-Orozco,[a] Victoria Bracamonte,[c] Elías Pérez,[a] Carla Bittencourt,[d] and Mildred Quintana*[a,e]

Graphene oxide-gold nanoparticle (AuNP@GO) hybrids were fabricated in water dispersions of graphene oxide (GO) and Au precursor completely free of stabilizing agents by UV-light irradiation. Gold nanoparticles (AuNP) nucleation, growth, and stabilization mechanisms at the surface of GO are discussed on the basis of UV-Vis, Raman, IR, and X-Ray photo-spectroscopy studies. The analyses of AuNP@GO hybrids by transmission electron microscopy (TEM), thermo gravimetric (TGA) and electrochemical tests exhibit outstanding chemical, thermal and electrochemical stabilities. Thus, AuNP@GO biosensing platforms were fabricated for surface enhanced Raman spectroscopy (SERS) detection of Crystal Violet (CV) a SERS standard molecule, and in a different set of experiments, for flavin adenine dinucleotide (FAD) a flavoprotein coenzyme that plays an important role in many oxidoreductase and reversible redox conversions in biochemical reactions. AuNP@GO hybrids synthesized by using UV light irradiation show exceptional stability and high intensification of the Raman signals exhibiting high potential as biomedical probes for detection, monitoring, and diagnosis of medical diseases.

Introduction

Graphene oxide (GO) is a promising material for the development of new advanced biological applications since it is easily incorporated into composites and hybrid materials. The oxygenated functional groups of GO, such as epoxide, alcohol, carboxylic acid, ketone, and aldehyde provide excellent aqueous dispersibility and numerous sites to covalently anchor biochemical functionalities increasing its biocompatibility.[1] Additionally, the large surface area of GO, including the reminiscence hydrophobic zones from graphene, allows the adsorption of organic aromatic molecules,[2] polymers,[3] and ions[4] by π-π stacking, hydrogen bonding (H-bond) and electrostatic interactions. These properties made GO a suitable material for the construction of biocatalytic platforms. For example, GO was used as support for the deposition of Pt-Ru nanoparticles (NP) for the electro-oxidation of methanol and ethanol[5] and GO-AuNP hybrids were produced for the construction of a glucose biosensor with high sensitivity and good stability.[6]

GO has been proposed as an excellent platform for surface enhanced Raman spectroscopy (SERS) by itself[7] or combined with the electromagnetic enhancement generated by the surface plasmon of metal NP of different sizes and morphologies.[8,9] Raman spectroscopy is a promising technique for biological detection since it comprises high sensitivity, label free detection, low sample volumes, low cost-instruments and real time detection.[10,11] Unfortunately, Raman spectroscopy of biomolecules is often limited by the lack of molecular stability under laser irradiation accompanied by high fluoresce molecular emission that masks the Raman signals. In this direction, GO has demonstrated excellent abilities as fluoresce quencher and molecule stabilizer[12] making GO-metal NP hybrids promising platforms for early medical diagnosis and monitoring of diseases by SERS.[13]

To achieve innovative SERS or any other type of biocatalyst platforms, it is extremely important to control the chemical synthesis of stable and reproducible GO-metal nanohybrids. GO is a non-stoichiometric compound, the chemical and physical properties of GO such as composition, size and morphology depend on the graphitic starting material, the methodologies used for the oxidation of graphite, the reduction of GO, *i.e.* chemical,[14] or microwave reduction,[15] among others. In addition, GO-metal NP platforms are synthesized using different reducing agents[16,17] and stabilizing

[a] Instituto de Física, Universidad Autónoma de San Luis Potosí, Manuel Nava 6, Zona Universitaria, San Luis Potosi, SLP 78290, Mexico.
E-mail: mildred@ifisica.uaslp.mx
[b] Graphenemex S.A. de C.V. Añil 345, Col. Granjas Mexico, Del. Iztacalco, CDMX 08400.
[c] Facultad de Matemática, Astronomía, Física y Computación (FaMAF). Universidad Nacional de Córdoba. IFEG, CONICET. Medina Allende s/n, Ciudad Universitaria, Córdoba, Argentina.
[d] Chemie des Interactions Plasma-Surface. University of Mons, Avenue Nicolas Copernic, 1, 7000 Mons, Belgium.
[e] Microscopia de Alta Resolución, Centro de Investigación en Ciencias de la Salud y Biomedicina, Universidad Autónoma de San Luis Potosí, Av. Sierra Leona 550, 78210, San Luis Potosí, SLP, México.

View Article Online
DOI: 10.1039/C7CP04817C

molecules[18,19] modifying the chemical environment at the surface and in consequence its performance during sensing protocols.[20] In addition, the presence of molecular additives might compromise the stability of GO-metal nanohybrid platforms in acidic, basic or ionic chemical environments where biochemical reactions usually take place.

In the present work, AuNP were attached to GO by the reduction of $HAuCl_4$ using UV light irradiation as reducing agent in aqueous media free of stabilizing agents. AuNP@GO hybrids show high density of AuNP well dispersed on the entire GO surface. The nanohybrid owns increased chemical, thermal, and electrochemical stabilities making it an excellent platform for biodetection. The SERS properties of AuNP@GO were evaluated for: i) crystal violet (CV) a standard molecule for SERS, and for ii) flavin adenine dinucleotide (FAD), a coenzyme present in numerous redox processes of metabolic reactions and biological electron transport. AuNP@GO hybrids exhibit highly reproducible enhanced SERS signals for CV and FAD revealing a great potential as sensing platform for the monitoring and early diagnosis of medical diseases in biological conditions.

Experimental

Materials and reagents

All reagents were purchased from Sigma-Aldrich and used without further purification. Milli-Q water (18.2 MΩ cm) was used in all the experiments. Graphite was purchased from Bay Carbon, Inc. (SP-1 graphite powder, batch N° 04100, lot. N° 011705, www.baycarbon.com), gold (III) chloride solution at 30% in dilute HCl (99.99% trace metals basis, Aldrich) was used as a metal precursor. HCl, NaOH, and commercially available 50 mM buffers of Tris, HEPES and Citrate were used to evaluate the chemical stability of the hybrid at 25 °C.

Characterization techniques

The optical absorbance of the samples was measured by UV-Vis spectroscopy with a Cary 60 spectrophotometer using 10 mm path length quartz cuvettes. Transmission electron microscopy (TEM) images were acquired on a TEM JEOL JEM-2100, using an accelerating voltage of 200 kV. Samples were prepared by drop casting of stable dispersions onto a TEM grid (200 mesh, cooper, carbon only). Scanning electron microscopy (SEM) images were acquired using a SU8020 Microscope from Hitachi equipped with a detector for backscattered and secondary electrons for SEM images; a typical operating voltage of 30 kV was used to acquire the images. Attenuated total reflectance-Fourier transform infrared spectroscopy (ATR- FTIR) was performed using a spectrometer Nicolet Nexus 470 FTIR (Nicolet, Madison, WI, USA). The interferograms covering a spectral range at a resolution of 80 scans, were collected at room temperature. The analyses of the spectral band regions were performed with the OMNIC E.S.P.5.1 software (Nicolet). The chemical composition of the samples was investigated by X-Ray photoelectron spectroscopy (XPS) using an XPSVERSAPROBE PHI 5000 from Physical Electronics, equipped with a Monochromatic Al Kα X-ray in UHV conditions. The energy resolution was 0.7 eV. For the compensation of built-up charge on the sample surface during the measurements, a-dual beam charge neutralization composed of an electron gun (~1 eV) and the argon ion gun (≤10 eV) was used. The XPS spectra were deconvoluted into different chemical surroundings using commercially available software (CASA-XPS). Thermo-gravimetric analysis (TGA) was performed on a TGA Q500 (TA instruments), under N_2 and air atmospheres, by equilibrating at 50°C, and following a ramp at 10°C/min up to 800 °C (approximately 1 mg of each compound). Surface enhanced Raman scattering (SERS) was measured with a Thermo Scientific DXR Raman Microscope equipped with a Diode–pumped solid-state laser (DPSS) at wavelength of 532 nm as excitation source. A 10 X objective with a 50 µM slit aperture and 5 s of exposure time and laser power of 10 mW. The samples were recorded from drops of the dispersions deposited over clean silicon wafers and left dry under vacuum.

Preparation of AuNP@GO hybrids

Graphite was oxidized using the improved Hummer´s method reported by Marcano et al., 2010.[21] A complete characterization of GO is reported in the Electronic Supporting Information (ESI). The deposition of AuNP on the surface of GO was made by the photoreduction of $HAuCl_4$ as metal precursor under UV light irradiation as reported by Quintana et al., 2010.[22] Briefly, 1 mg of GO was dispersed into 80 mL of methanol-deionized water solution (1M) and mixed with $HAuCl_4$ at different molarities (0.12, 0.25, 0.37, 0.50 and 0.62 mM $HAuCl_4$). The mixtures were irradiated with UV light (GE.R 500 W Helios Italquartz, UVB, UVA ozone free emission 310-450 nm, λ_{max}= 360 nm) for 60 min under magnetic stirring. Products were thoroughly washed by vacuum filtration and dispersed in fresh solvent and fully characterized (see ESI). The sample prepared at 0.37 mM of $HAuCl_4$ was further evaluated since smaller size distribution of AuNP was found for this concentration.

Electrochemical analysis

Cyclic voltammetry measurements were carried out at room temperature using an Autolab potensiostat/galvanostat (Model 302N). A conventional 3 electrodes cell was used for all the measurements using a Glassy Carbon Electrode (Model 101, CH Instruments, GCE) as working electrode, Ag/AgCl (NaCl, 3M) (Model 111, CH Instruments) electrode as reference and a Pt wire as counter electrode. Prior to their use, the glassy carbon electrodes were cleaned by mechanical polishing using 1.0 µm and 0.3 µm alumina slurry (micropolish Buehler) for 2 min, following by sonication in deionized water for 30 s and rinsed with ultrapure water. The modification of the GCE surface with AuNP@GO was done by drop casting using 20 µL of the AuNP@GO dispersion and drying it for 20 min at 323 K. The resulting electrodes are labeled GCE/AuNP@GO. All the measurements were performed 5 times and average results are presented.

SERS probes

SERS experiments were prepared from aqueous dispersions under diluted conditions. AuNP@GO hybrid dispersion was

View Article Online
DOI: 10.1039/C7CP04817C

mixed (1:1 v/v) with the model analyte VC (1X10^{-6} M) dissolved in water and FAD (1X10^{-6} M) in phosphate buffer saline (PBS) solution. Mixed dispersions were deposited on cleaned silicon oxide substrates and allowed to dry under ambient conditions. GO and AuNP controls were measured at the same experimental conditions; results are reported in the ESI. The mixture was left to stabilize overnight in darkness at room temperature.

Results and discussion

The selective functionalization of single walled carbon nanotubes (SWCNT) with AuNP by UV light irradiation was reported showing that oxidized defects on the carbon skeleton of SWCNT are required for the nucleation, formation and stabilization of AuNP.[22] However, regarding to the interaction of carbon nanostructures with light there are several differences between SWCNT and GO: SWCNT are a highly curved carbon nanomaterial compared with the relatively flat surface of GO. Curvature is directly related to the electronic structure and chemical reactivity, as higher curvature, higher reactivity.[23] Instead, graphene and GO are two dimensional surfaces with two available sides for chemical functionalization allowing cooperative reactions to occur.[24] Moreover, GO is a highly oxidized surface compared with oxidized SWCNT, in consequence GO is considered an insulator material[25] while SWCNT are semiconductor or metallic depending on the diameter and chiral vector.[26] For CNT, it was observed higher nucleation of AuNP on metallic SWCNT associated with the higher probability of electron-hole pair formation. For highly oxidized SWCNT, the growing of AuNP was not observed.
Despite the differences in the physical and chemical properties of GO and SWCNT, GO was easily functionalized with AuNP by UV light irradiation. In the next paragraphs, the nucleation, growth, and stabilization mechanisms are explained based on the spectroscopic characterization of the hybrid. These characterization techniques explain the chemical, thermal, and electrochemical stability of the AuNP@GO hybrids.

Spectroscopic and electron microscopy analyses

In Fig. 1 the UV-Vis spectra of GO, AuNP and AuNP@GO are shown. For the GO spectra, two signals are observed, one at 231 nm coming from the π-π transition of C-C and C=C bonds in sp^2 plane and a shoulder peak at 303 nm corresponding to the n-π transitions of the C=O bond in sp^3 regions.[27] As control experiment, we performed the synthesis of AuNP in the same experimental conditions lacking of GO. AuNP dispersions present two signals, a strong and broad peak around at 520 nm attributed to the localized surface plasmon resonance (LSPR) and the second band at 257 nm coming from the transition of electrons from the occupied d-level states to empty states in the conduction band above the Fermi level.[28] The LSPR of AuNP@GO presents red shift of ~15 nm compared to the position displayed for AuNP. This shift is associated to the variation of the dielectric constant of the medium. AuNP in the nanohybrid are embedded in a surface and consequently are subject to an average polarization field.[29] Additionally, for the hybrid the signal at 260 nm is broader than the one observed for the AuNP. This result accounts for the contributions from the d-transition of the AuNP and the new electronic levels produced in the valence and conduction bands of GO.[30] Finally, the shoulder at 303 nm, related to GO sp^3 transitions is missing in the nanohybrid evidencing a strong interaction between the AuNP and GO sheets.

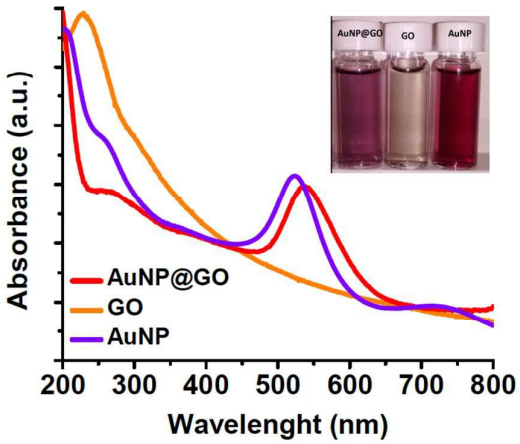

Fig. 1. UV-vis spectra of GO (orange), AuNP (violet), and AuNP@GO hybrid (red). The inset photograph shows the different colour of the stable dispersions of GO, AuNP, and AuNP@GO hybrids.

Fig. 2a shows a TEM micrograph of the AuNP@GO nanohybrid. The image displays GO sheets with high concentration of AuNP well dispersed at the edges and all over the basal planes. The average size distribution of the spherical AuNP is 24 ± 7 nm, Fig. 2b. At higher magnification, Fig. 2c, miscellaneous AuNP morphologies as pyramidal, triangles, rods and icosahedral NP well distributed on the GO surface are observed. The growth of different size and forms of AuNP has been related with the nature and the amount of oxidized defects present on the GO surface. On these defects it is expected the NP nucleation to take place.[18,31] In Fig. 2d a scanning transmission microscopy (SEM) image of deposited AuNP@GO hybrid shows a high density of AuNP hindering the aggregation of GO sheets and allowing good coverage of the silicon oxide surface.
Attenuated total reflectance Fourier transform infrared spectroscopy (ATR- FTIR) for GO reported in Fig. 3 shows a prominent absorption band between 2500 and 3500 cm^{-1} corresponded to the hydroxyl groups (–OH). The broad series of peaks in the range between 1840–840 cm^{-1} are conformed by: C=O (□1713 cm^{-1}), C=C aromatic (□1611 cm^{-1}), tertiary alcohol bending (□1372 cm^{-1}), phenolic groups [Ar–OH (1278 cm^{-1})], bending and asymmetric stretching modes of the epoxygroup [C–O–C (850 and 1220 cm–1)] and the alkoxy vibrations [C–O (1060 cm^{-1})].[32]

View Article Online
DOI: 10.1039/C7CP04817C

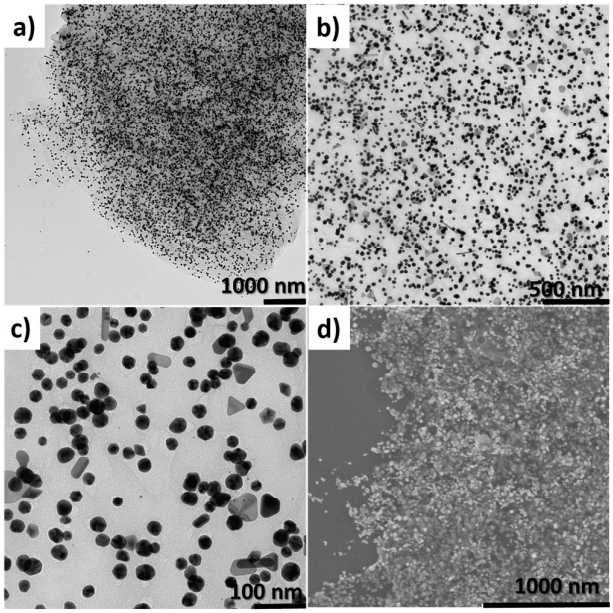

Fig. 2. a), b) and c) TEM and d) SEM micrographs of AuNP@GO hybrid at different magnifications. AuNP of different morphologies are observed, c).

After NP growth by UV light, the characteristic features of GO are not longer observed implying a reduction on the vibration modes of the oxygen functionalities in AuNP@GO. This observation could result either from the reduction of the oxygenated moieties or from the anchoring of the AuNP on top of them hindering vibration modes. Similar results have been reported for the UV assisted photocatalytic reduction of GO by semiconductor NP such as TiO_2[33] and ZnO.[34]

Fig. 4 a) shows the XPS spectra of the C 1s peak recorded for GO. The main characteristic peaks of GO are found at 284.5 eV (C=C, 64.29%), 286.7 eV (C-O, 32.84%) and 288.6 eV (O-C=O, 2.87%). Fig. 4 b) shows the C 1s spectra for AuNP@GO hybrid. Two new signals appear at 296.2 eV (C 1s, 3.26%) and 293.3 eV (C 1s, 3.24%). These bands are related to localized aromatic sp^2 structures and a π-π shake up band attributed to the partial restoration of the aromaticity of the graphene sheets.[35] The rest of the signals present a small shift originated from the change on the chemical environment. 283.2 eV (COOH, 8.65%), 288.8 eV (O-C=O, 10.32%), 286.9 eV (C-O, 18.00%), 285 eV (C=C, 58.61%). Comparison of the line shapes of the C 1s XPS spectrum recorded after the Au deposition shows that the C 1s satellite peaks due to oxygenated-groups are reduced. As for the IR characterization, two effects can contribute to this observed signals reduction. First photoelectrons emitted from C atoms under AuNP will experience inelastic losses when passing through the metal, and thus no longer contribute to the C 1s main peak. If AuNP selectively cover oxygen-rich areas, thus the intensity from oxygen-related C 1s satellite peaks will be selectively reduced. A second possible source for the reduction in oxygen-related C 1s satellite peaks is the formation of O-Au bonds. C-O-Au bonding will change the screening of the C-O bonds thereby changing the binding energy of their C 1s levels.

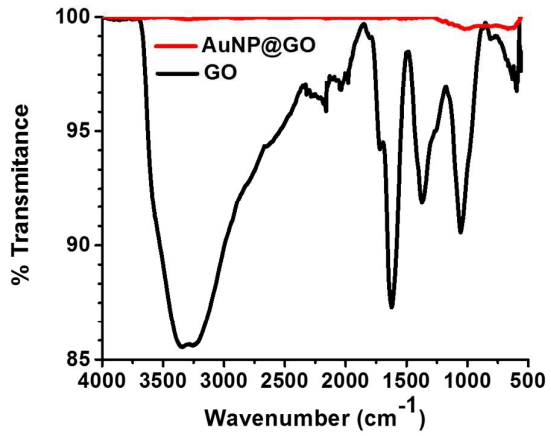

Fig. 3. ATR-FTIR of GO and AuNP@GO.

Fig. 4 c) shows the binding energy of the major component of Au 4f. The Au 4f7/2 peak appeared at a binding energy of 84.3 eV and the Au 4f5/2 peak appeared at 87.9 eV corroborating the binding of AuNP.[35]

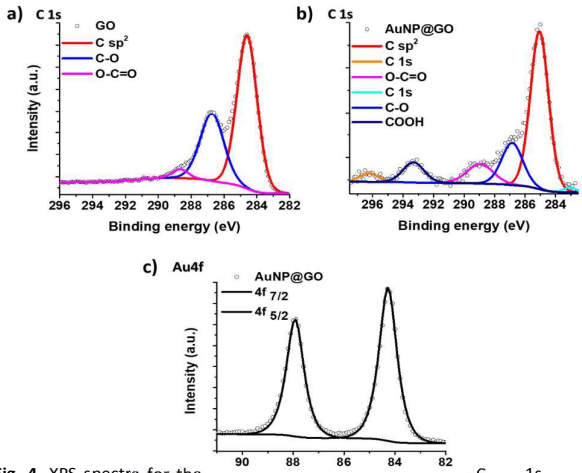

Fig. 4. XPS spectra for the C 1s peak recorded on a) GO and b) AuNP@GO. XPS analysis spectra for the 4f peaks recorded on AuNP@GO.

Raman spectra of GO and AuNP@GO presented in Fig. 5 show two characteristic peaks located at 1347 and 1584 cm^{-1}, are attributed to D and G bands, respectively. The D bands correspond to a defect induced in plane A_{1g} zone-edge mode while the G band is attributed to E_{2g} vibrational modes of sp^2 orbitals and their domains. After AuNP photo-deposition, the D and G bands red shifted to 1356 and 1606 cm^{-1}, respectively, and the intensity ratio (I_D/I_G) changed from ~ 1.0 to 0.94 for the AuNP@GO nanohybrid, indicating a decrease in the size of the sp^3 domains. The 2D band at ~2700 cm^{-1}, which originates from a two phonon double resonance Raman process is indicative of crystalline graphitic materials. The position and

View Article Online
DOI: 10.1039/C7CP04817C

shape of the 2D band are highly sensitive to the number and thickness of graphene layers. The AuNP@GO nanohybrid exhibits two bands close to 2700 and 2930 cm^{-1} corresponding to the 2D band and to a (D+G) combination mode induced by disorder. These features, namely the emergence of a 2D and a lower intensity distinguishable D+G bands, support better graphitization in the nanohybrid compared to GO.[36] AuNP@GO spectrum indicates the reduction of the oxidized carbon components.[37]

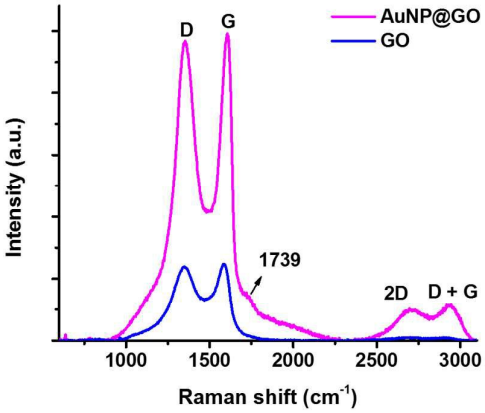

Fig. 5. Raman spectra of GO and AuNP@GO nanohybrid. The spectra consists of D, G, 2D and D + D´ bands located at 1347, 1585, 1739, 2718, and 2930 cm^{-1}, respectively.

Several studies have shown that Au atoms interact weakly with graphene sheets making the density of defects at the carbon skeleton the principal responsible for metal NP growth and stabilization.[38] Our results from spectroscopic characterization indicate that AuNP grown on GO involves the combination of 4 different effects: (i) electrostatic interactions between Au ions where GO surface guide them to a strong immobilization on the carbon structure; this process is followed by (ii) the reduction of the anchored Au ions by UV light irradiation; then (iii) the π-electron aromatic system found in GO interacts with the d-orbitals of the AuNP producing their stabilization;[39] and finally, (iv) the covalent attachment of AuNP on oxygenated functional groups accounts for the selective distribution of NP at the defects in GO.[40] Importantly, the difference on the chemical nature and density of oxygenated functional groups produce AuNP of different sizes and morphologies. It is well known that hot spots, necessary for SERS, are strongest in anisotropic NP. All these events allow the production of AuNP free of stabilizing agents improving the AuNP surface activity due to the absence of ligands.

Chemical, thermal and electrochemical stability analyses

To evaluate the chemical stability, AuNP@GO hybrids were dispersed in aqueous solutions with different ionic strength (50 mM TRIS, HEPES and citrate buffers). In a different set of experiments, the stability of the hybrids was evaluated at different pH, raging from 1 to 12. All the experiments were performed at 25 °C. TEM micrographs demonstrate that AuNP stay attached to the GO surface in ionic, acidic and alkaline conditions. These results are important as the chemical stability of GO-metal NP depends on the protocol used for its synthesis. Often, thermal and oxidative treatments are used to remove stabilizing agents, changing the size and morphology of metal NP altering their catalytic activity.[41] Some mechanisms of NP stabilization are based on electrostatic interactions producing the release of NP under certain ionic or pH conditions.[42] The AuNP growth on GO by UV light irradiation lacking of capping agents exhibits a strong NP anchoring in a wide range of chemical environments. The formation of C-O-Au bonds confirmed by UV-Vis, ATR-FTIR, XPS and Raman spectroscopies explain the chemical stability observed for the AuNP@GO hybrids.

Fig. 6 shows the thermographs for GO and AuNP@GO in air and N_2 atmospheres up to 800 °C. Under air, Fig. 6 a) shows that at ~200 °C most of the water molecules attached by H-bonds to the GO surface are eliminated. The largest weight loss at ~ 550 °C is due to the oxidation of C atoms starting at the already oxygenated functionalities.[22] Instead, for AuNP@GO the solvent was completely eliminated by the previous vacuum drying of the samples. The presence of AuNP on GO hindered the H-bond formation and prevents the oxidation of the GO lattice as indicated by the 88 wt. % of AuNP@GO hybrid preservation at 800 °C. Under N_2 atmosphere, shown in Fig. 6 b) the thermal stability of both products increases; in this case, it is interesting to note that the AuNP@GO hybrid maintains almost the same thermal stability in air than in N_2 indicating the absence of oxygenated functional moieties where further oxidation usually initiates. These results support that AuNP are covalently attached on the oxygenated defects, providing thermal stability to GO.

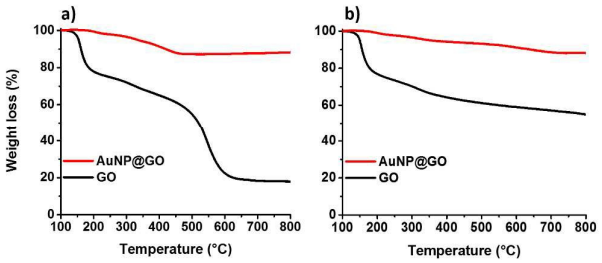

Fig. 6. TGA for GO and AuNP@GO hybrid in a) air and b) N_2 atmospheres up to 800 °C.

AuNP@GO hybrid was further exanimated by electrochemical measurements in N_2 saturated 0.50 M H_2SO_4 solution using GC electrodes modified with AuNP@GO hybrid. The electrochemical response, reported in Fig. 7, evidences the presence of two peaks: a broad one during the anodic scan (starting at ca 1.05 V) and another on the cathodic scan (at ca 0.88 V), corresponding to the oxidation and reduction of AuNP, respectively. From the voltammetric profiles, the electroactive

View Article Online
DOI: 10.1039/C7CP04817C

surface area of gold (EASA) was determined using the charge integration under the oxide reduction peak, and employing the equation,

$$A = \frac{Q_{red}}{420\,\mu C\,cm^{-2}}$$

where 420 μC cm^{-2} is the necessary charge to reduce a monolayer of gold oxide on a polycrystalline surface. The calculated area was (0.023 ± 0.002) cm^2 evidencing an electroactive surface area which represents the 30 % of the geometric area (0.07 cm^2).

The stability of the signal after several oxidation-reduction cycles was evaluated. For the analysis, the signal was normalized considering the cathodic charge of the first cycle as 100 % of response. The results, presented in the inset of Fig 7, show no significant changes after 10 cycles, evidencing a non-deactivation or leaching of the gold nanostructures during the cycling treatment directly related with the robustness of the system.

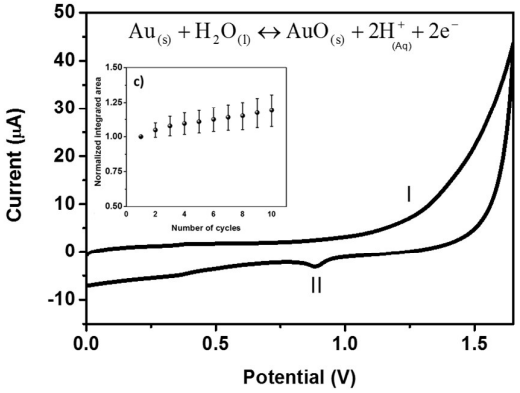

Fig. 7. Electrochemical response and stability of AuNP@GO hybrid.

The aging of metal NP on carbon supports is an important parameter in the design of chemical and electrochemical biosensors. The predominant degradation mechanism of supported metal NP on carbon materials involves the migration/aggregation of the metal NP due to chemical or electrochemical reduction and the detachment of the metal NP in oxidizing environments like those present in certain type of diseases.[43] As we discussed previously, the Au reduction by UV light irradiation simultaneously promotes the GO reduction forming C-O-Au bonds by electron transfer. This mechanism results in highly stable AuNP@GO hybrids within different chemical environments and electrochemical processes. Our results demonstrate that GO is an excellent substrate for the growth of AuNP in water dispersions by UV light irradiation. Photo-induced ligation of NP has been proposed as a very versatile strategy for processing NP and to produce reactive nanocrystals.[44] The presence of oxygenated defects distributed on the carbon skeleton of GO is adequated for the transfer of electrons necessary for the Au reduction and covalent anchoring of NP on the GO surface producing highly stable AuNP@GO hybrids in different chemical and electrochemical environments at relevant temperature.

AuNP@GO platforms for SERS detection

CV was probed as a model analyte, for this, aliquots of CV, AuNP-CV, GO-CV, and AuNP@GO-CV (CV, 500 nM) were deposited on bare SiO_2/Si substrates with the same surface area and dried under vacuum. The sample preparation allows the complete mixing of the sensing and the analyte species. Then, in order to test the reproducibility of the detection system, the measurement was performed in 5 different substrates prepared under the same experimental conditions.

Raman spectra are shown in fig. 8a). The AuNP@GO-CV spectrum exhibits a strong enhancement and better definition of the vibrational bands at ~ 726, 806, 916, 1182, 1370, 1617 cm^{-1} characteristics of CV (see ESI). The contributions of SERS by both chemical and electromagnetic components are evident in the AuNP@GO-CV spectra when compared with AuNP-CV and GO-CV, as shown in ESI.

The chemical effect is supported by the small shift in the active Raman modes of CV on AuNP@GO platform compared with CV Raman spectrum.[9] The enhancement factor (EF) of the AuNP@GO platform was calculated according to the following relation:

$$EF = (I_{SERS}/N_{ads})/(I_{bulk}/N_{bulk})$$

where I_{SERS} and I_{bulk} are the intensities of a selected vibration mode in the SERS spectra and in the Raman spectra, respectively. N_{ads} and N_{bulk} are the number of molecules in the SERS and Raman spectrum.[1] The EF obtained for AuNP@GO hybrid is 1.5 X 10^3 with a limit of detection of 10^{-10} M (See ESI). Finally, to assess the effectiveness of the AuNP@GO hybrid for biological probes, the coenzyme FAD was evaluated. In this case, the AuNP@GO-FAD spectra exhibit a strong enhancement and better definition of the vibrational bands at ~ 1066, 1156, 1226, 1347, 1404, 1453, 1497, 1539, 1577, 1625 cm^{-1} characteristics of FAD (see ESI) as shown in Fig. 8b. As observed for CV, many characteristic bands of FAD are shifted, probably due to a charge-transfer effect. Besides, the Raman enhancement turns out to be cleaner and reproducible with a calculated EF of 1 X 10^4 and a limit of detection of 10^{-9} M (see ESI). This enhancement can be attributed, in part to GO, since displays SERS effects making the system more stable against laser-induced damage such as photocarbonization and photobleaching adsorbing FAD molecules on its surface. A remarkable less enhancement was observed for AuNP or GO alone at the same experimental conditions demonstrating the importance of the hybrid platform. Thus, the stability of AuNP@GO hybrids sets the distribution of the molecules and states more stable in the vicinity of the electromagnetic hot

View Article Online
DOI: 10.1039/C7CP04817C

spots produced by AuNP collected on a flat GO surface. This synergy effect between GO and AuNP provides higher sensitivity compared to traditional SERS effect.

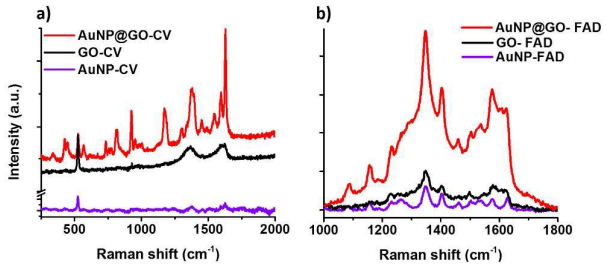

Fig. 8. Surface enhanced Raman spectroscopy on AuNP@GO platform for a) Crystal Violet (CV) and b) Flavin Adenine Dinucleotide (FAD).

Conclusions

In this work, a straightforward methodology for the production of AuNP@GO platforms for SERS applications is reported. UV light irradiation was applied to water dispersions of GO and Au precursor inducing the selective reduction Au ions on top of oxygenated functional moieties of GO. AuNP of different sizes and morphologies were strongly anchored to the GO surface producing AuNP@GO hybrids owning excellent chemical, thermal, and electrochemical stability. Then, AuNP@GO hybrids were proved as SERS templates showing a significant enhancement of the Raman signals of CV, a standard SERS probe molecule, and in a different set of experiments for FAD, a coenzime in many oxidoreductase and reversible redox conversions for biochemical reactions. The Raman enhancement results from the synergy between the unique properties of GO and AuNP. GO is an amphiphilic surface with the ability to absorb large amounts of organic and biological molecules producing fluorescence quench and stabilization of the biomolecules under laser irradiation. Additionally, GO used as template controls the spatial localization of AuNP assembling surface plasmon resonances in hotspots necessary for SERS. The different morphology of NP produced by the diversity of oxidized carbon functionalities on GO accounts for SERS since higher production of plasmon resonances is associated to non-spherical NP. The AuNP@GO are chemically, thermally and electrochemically stable, thus it is expected to contribute to the development of advanced SERS biosensors in relevant biological conditions.

Conflict of interest

There are no conflicts to declare.

Acknowledgements

This research was supported by CONACYT through the projects PN-1767, I-225984. Thanks are given to Mons University for financial support. DHJ thanks Conacyt for the PhD scholarships number 23755. We are grateful to Dra. Aurora Robledo, and M.C. Lourdes González-González for technical support.

Notes and references

1 M. Xu, J. Zhu, F. Wang, Y. Xiong, Y. Wu, Q. Wang, J. Weng, Z. Zhang, W. Chen and S. Liu, *ACS Nano*, 2016, **10**, 3267–3281.
2 D. Hernández, M. Scardamaglia, S. Saucedo-Anaya, C. Bittencourt, M. Quintana, *RSC Adv.,* 2016, **6**, 66634- 66640.
3 J. Zhang and X. S. Zhao, *J. Phys. Chem.* C, 2012, **116**, 5420-5426.
4 G. Zhao, J. Li, X. Ren, C. Chen, and X. Wang, *Environ. Sci. Technol.,* 2011, **45**, 10454–10462.
5 L. Dong, R.R.S. Gari, Z. Li, M. M. Craig, S. Hou, *Carbon,* 2010, **48**, 781-787.
6 Y. Song, K. Qu, C. Zhao, J. Ren, X. Qu, *Adv. Mater.*, 2010, **22**, 2206-2210.
7 K. Yu, K. L. Kelly, N. Sakai, and T. Tatsuma*, Langmuir* 2008, **24**, 5849-5854
8 J. Lee, J. Kim S. Kim, D-H. Min, *Adv. Drug Deliver. Rev.,* 2016, **10***5*, 275- 287.
9 C. Chung, Y-K. Kim, D. Shin, S-R Ryoo, B. H. Hong, D-H. Min, *Acc. Chem. Res.*, 2013, **46**, 2211–2224.
10 T. Van Dijk, S.T. Sivapalan, B.M. DeVetter, T.K. Yang, M.V. Schulmerich, R. Murphy, C.J. Bhargava, P.S. J. Carney, *Phys. Chem. Lett.,* 2013, **4**, 1193- 1197.
11 S.T. Sivapalan, B.M. DeVetter, T.K. Yang, T. Van Dijk, M.V. Schulmerich, P.S. Carney, R. Bhargava, C.J. Murphy, *ACS Nano*, 2013, **7**, 2099- 2105.
12 K. P. Loh, Q. Bao, G. Eda, and M. Chhowalla, *Nat. Chem.*, 2010, **2**, 1015-1024.
13 D. Lin, T. Qin, Y. Wang, X. Sun, L. Chen, *ACS Appl. Mater. Interfaces*, 2014, **6**, 1320−1329.
14 S. Stankovich, D. A. Dikin, R. D. Piner, K. A. Kohlhaas, A. Kleinhammes, Y. Jia, Y. Wu, S, T. Nguyen, R. S. Ruof, *Carbon*, 2007, **45**, 1558- 1565.
15 W. Chen, L. Yan, PR. Bangal, *Carbo*n, 2010, **4**, 1146-1151.
16 Y. Guo, X. Sun, Y. Liu, W. Wang, H. Qiu, J. Gao, *Carbon,* 2012, **50**, 2513- 2523.
17 J. Liu, S. Fu, B. Yuan, Y. Li, Z. Deng, *J. Am. Chem. Soc*., 2010, **132**, 7279- 7281.
18 J. Huang, L. Zhang, B. Chen, N. Ji, F. Chen, Y. Zhang, Z. Zhang, *Nanoscale*, 2010, **2**, 2733-2738.
19 A.J. Patil, J. L. Vickery T. B. Scott, S. Mann, *Adv. Mater.* 2009, **21**, 3159- 3164.
20 J. Liang, Z. Chen, L. Guo, and L. Li, *Chem. Commun.* 2011, **47**, 5476-5478.
21 D. C. Marcano, D. V. Kosynkin, J. M. Berlin, A. Sinitskii, Z. Sun, A. Slesarev, L. B.Alemany, W. Lu, J. M. Tour, *ACS Nano*, 2010, **4**, 4806- 4814.
22 M. Quintana, X. Ke, G. Van Tendeloo, M. Meneghetti, C. Bittencourt, M. Prato, *ACS Nano,* 2010, **4**, 6105-6113.
23 Z. Chen, W. Thiel, A. Hirsch, *Chem. Phys. Chem*., 2003, **4**, 89-93.
24 P.A. Denis, F. Iribarne, *Chem. Phys. Lett.* 2012, **550**, 111-117.
25 D. R. Dreyer, S. Park, C. W. Bielawski, R. S. Ruoff, *Chem. Soc. Rev.* 2010, **39**, 228-240.
26 S. J. Tans, A. R. M. Verschueren, and C. Dekker, *Nature,* 1998, **391**, 62-64.
27 B. Balamurugana, and T. Maruyama, *Appl. Phys. Lett.* 2005, **87**, 143105- 1.
28 K. L. Kelly, E. Coronado, L. L. Zhao and G. C. Schatz, *J. Phys. Chem. B,* 2003, **107**, 668-677.
29 K. Yu, K. L. Kelly, N. Sakai, and T. Tatsuma, *Langmuir,* 2008, **24**, 5849-5854.

View Article Online
DOI: 10.1039/C7CP04817C

30 A. Mathkar, D. Tozier, P. Cox, P. Ong, C. Galande, K. Balakrishnan, A.L.M. Reddy, and P.M. J. Ajayan, *Phys. Chem. Lett*., 2012, **3**, 986-991.
31 G. D. Barmparis, Z. Lodziana, N. Lopez, I. N. Remediakis, *Beilstein J. Nanotechnol.* 2015, **6**, 361-368.
32 G. Williams, B. Seger, PV. Kamat, *ACS Nano,* 2008, **2**, 1487-1491.
33 X. Liu, L. Pan Q. Zhao, T. Lu, G. Zhu, T. Chen, T. Lu, Z. Sun, C. Sun, *Chem. Eng. J.* 2012, **183**, 238-247.
34 G. Zhang, S. Sun, D. Yang, J. P. Dodelet, E. Sacher, *Carbon*, 2008, **46**, 196-205.
35 H.G. Boyen, A. Ethirajan, G. Kästle, F. Weigl, P. Ziemann, G. Schmid, M.G. Garnier, M. Büttner, P. Oelhafen, *Phys. Rev. Lett.,* 2005, **94**, 016804/1-4.
36 S. Karna, M. Mahat, T-Y. Choi, R. Shimada, Z. Wang, A. Neogi, Sci. Rep. 2016, **6**, 1-11.
37 P. Kar, S. Sardar B. Liu, M. Sreemany, P. Lemmens, S. Ghosh, and S.K. Pala, *Sci. Technol. Adv. Mater.* 2016, **17**, 375–386.
38 C. Bittencourt, A. Felten, B. Douhard, J. Ghijsen, R.L. Johnson, W. Drube, J.J. Pireaux, *Chem. Phys.,* 2006, **328**, 385–391.
39 V. Pérez-Luna, S. Oros-Ruiz, E. Pérez, M. Quintana, *Phys. Status Solidi B*, 2017, **DOI:** 10.1002/pssb.201700187.
40 R. Torres, D. Ventura, S. Sabater, J. Lancis, G. Mínguez, J. Mata, *Sci. Rep.* 2016, **6**, 30478.
41 J.A. Lopez, N. Dimitratos, C. Hammond, G.L. Brett, L. Kesavan L. White, S. Miedziak, P. Tiruvalam R. Jenkins R. L. Carley, A. F. Knight, D. Kiely, C. J. and G. J. Hutchings, *Nat. Chem.* 2011, **3**, 551- 556.
42 J. Della Rocca, D. Liu, and W. Lin, *Acc. Chem. Res.,* 2011, **44**, 957-968.
43 P. Jenner and C.W. Olanow, *Ann. Neuro*., 2014, **44**, S72-S84.
44 F. Aldeek, D. Hawkins, C. Palomo, M. Safi, G. Palui, P. E. Dawson, I. Alabugin, H. Mattoussi, *J. Am. Chem. Soc*., 2015, **137**, 2704-2714.

View Article Online
DOI: 10.1039/C7CP04817C

Highly Stable Graphene Oxide-Gold Nanoparticle Platforms for Biosensing Applications

Dania Hernández-Sanchez, Giovanny Villabona-Leal, Victoria Bracamonte, Elías Pérez, Carla Bittencourt, and Mildred Quintana

A straightforward, highly reproducible, and clean methodology yielding AuNP@GO hybrids with excellent chemical, thermal, and electrochemical stabilities for SERS biodetection is reported.